ChemComm

ROYAL SOCIETY OF CHEMISTRY

COMMUNICATION

View Article Online
View Journal | View Issue

Cite this: *Chem. Commun.*, 2022, **58**, 3354

Received 16th November 2021,
Accepted 7th February 2022

DOI: 10.1039/d1cc06456h

rsc.li/chemcomm

Bismuth-based mixed-anion compounds for anode materials in rechargeable batteries†

Prashant Kumar,[a] Wandi Wahyudi,[a] Abhinav Sharma,[a] Youyou Yuan,[b] George T. Harrison,[a] Murali Gedda,[a] Xuan Wei,[a] Abdulrahman El-Labban,[a] Shahzad Ahmad,[c] Vinod Kumar,[d] Vincent Tung[a] and Thomas D. Anthopoulos *[a]

A facile solvothermal synthesis approach for chemical composition control in ternary Bi–S–I systems is reported by simply controlling the sulfide concentration. We demonstrate the application of these bismuth-based ternary mixed-anion compounds as high capacity anode materials in rechargeable batteries. Cells utilising $Bi_{13}S_{18}I_2$ achieved an initial capacity value of 807 mA h g^{-1}, while those with BiSI/$Bi_{13}S_{18}I_2$ a value of 1087 mA h g^{-1} in lithium-ion battery systems.

Mixed-anion compounds are subjects of immense interdisciplinary interest compared to mono-anion compounds due to them inheriting properties of the different constituent anions in a single molecular material along with several new and interesting properties of additional orbital hybridization.[1–3] These properties can further be tuned by controlling the stoichiometry of the anions and charge rebalancing, thus finding potential applications in a wide range of fields, including electrical, magnetic, optical, energy storage and transport devices.[1,4] Bismuth sulfide iodide systems (Bi–S–I), a class of ternary mixed anion compounds, possess a quite complex phase diagram ranging from metastable/intermediate compositions,[5] along with thermodynamically stable phases of BiSI and $Bi_{19}S_{27}I_3$.[5–7] In particular, the structure of $Bi_{19}S_{27}I_3$ was debatable for a long time,[7] with the recent structural analysis by Groom *et al.*[8] referred to as $Bi_{12.67}S_{18}I_2$ or $Bi_{13}S_{18}I_2$ for the sake of convenience. It is noteworthy to mention that $Bi_{13}S_{18}I_2$ has a unique structure in which ribbon like subunits of $(Bi_4S_6)_\infty$, *i.e.*, $[(Bi_2S_3)_2]_\infty$, form six spokes around a central hexagonal channel at the corners of the unit cell.[8] BiSI and $Bi_{13}S_{18}I_2$ are termed as sulfur-deficient and sulfur-rich compositions depending on the sulfide stoichiometry present.

Bi_2S_3 has been regarded as a promising host for lithium-ion storage, but enormous volume expansion takes place upon the charging–discharging process, which leads to pulverization of the Bi_2S_3 particles, thus compromising its performance as an electrode for lithium-ion batteries (LIBs).[9,10] To overcome this crucial challenge, several Bi_2S_3-based composites have been introduced, such as yolk–shell Bi_2S_3@C, core–shell Bi_2S3@C, Bi_2S_3/C nanorods, Bi_2S_3–CNT, and Bi_2S_3–MoS_2.[9–14] Compared to a composite, using a molecular compound is advantageous because of its homogeneity, while components in the composite remain separate and distinct within the finished structure, which makes it relatively difficult to understand. Therefore, the exploration of inorganic/organic ternary mixed-anion compounds such as bismuth-based materials and their use as an integral part of battery electrodes are desirable.

Here, we present a facile synthesis of bismuth-based materials and demonstrate their applications as electrodes in LIBs. Our obvious choices of these ternary mixed-anion materials are $Bi_{13}S_{18}I_2$ and BiSI. Besides the aforementioned structural properties of $Bi_{13}S_{18}I_2$, BiSI possesses a layered structural arrangement that is also suitable for ion migration. In particular, the structure of the $[(BiSI)_\infty]_2$ ribbons in BiSI is held together by weak ionic or van der Waals-type forces.[7]

We employed BiI_3 as the molecular precursor for bismuth and iodine in place of using two separate precursors for each element, while thiourea was used as the source of sulfur. Both the precursors, *i.e.*, BiI_3 and thiourea, are quite stable compounds. To prevent the evolution of toxic gases, the reactions were performed under a closed atmosphere using ethanol as the reaction medium, as both the precursors show an excellent solubility in ethanol (see Experimental section, ESI†). In a typical synthesis of sulfur-rich bismuth sulfide iodide, *i.e.*, $Bi_{13}S_{18}I_2$, 4 mmol of thiourea was first mixed with 1 mmol of BiI_3 in an 82 mL autoclave using 60 mL of ethanol at 60 °C for 7 hours to ensure that both the compounds were well mixed

[a] *KAUST Solar Center, King Abdullah University of Science and Technology (KAUST), Thuwal 23955-6900, Saudi Arabia. E-mail: thomas.anthopoulos@kaust.edu.sa*
[b] *Core Labs, King Abdullah University of Science and Technology (KAUST), Thuwal 23955-6900, Saudi Arabia*
[c] *Department of Chemistry, Zakir Husain Delhi College, University of Delhi, Delhi 110002, India*
[d] *Special Center for Nanoscience, Jawaharlal Nehru University, Delhi 110067, India*

† Electronic supplementary information (ESI) available: Experimental details and additional results. See DOI: 10.1039/d1cc06456h

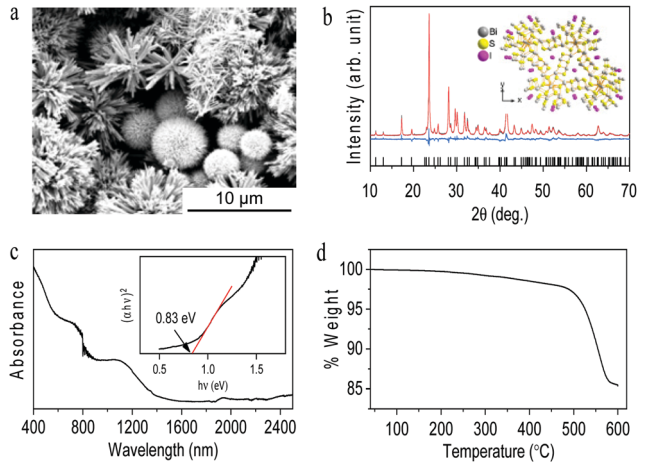

Fig. 1 (a) SEM image of the synthesized $Bi_{13}S_{18}I_2$. (b) XRD pattern of the synthesized triclinic $Bi_{13}S_{18}I_2$, with observed, calculated (profile matching), and difference profiles obtained by Rietveld refinement, shown as black, red, and blue lines; the Bragg positions are shown as black vertical lines. Inset: Structure of trigonal $Bi_{13}S_{18}I_2$. (c) Absorbance spectrum of the compound in the visible-NIR range; inset: band gap of the compound. (d) TGA analysis of the compound.

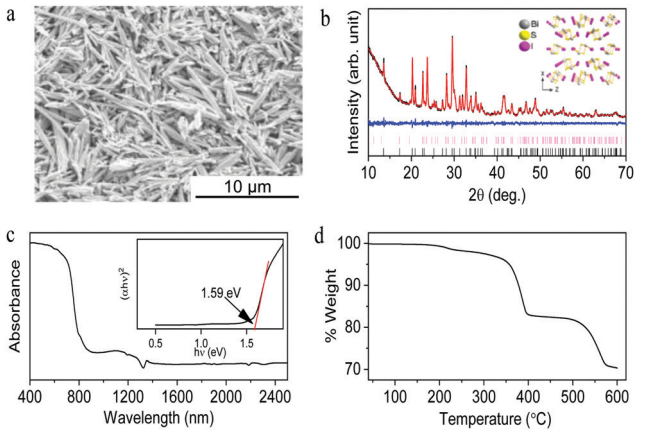

Fig. 2 (a) SEM image of the synthesized BiSI. (b) XRD pattern of the synthesized compound, with observed, calculated (profile matching), and difference profiles shown as black, red, and blue lines; the Bragg positions for BiSI and $Bi_{13}S_{18}I_2$ are shown as black and pink vertical lines, respectively. Inset: Structure of orthorhombic BiSI. (c) Absorbance spectrum of the compound in the visible-NIR range; inset: band gap of the compound. (d) TGA analysis of the compound.

and then the solution was heated at 120 °C for 24 hours. After the reaction, a black color compound was separated and washed several times using a centrifuge at 2000 rpm at room temperature and washed several times using ethanol and isopropanol followed by drying at room temperature. The morphologies of the synthesized particles were first observed by field emission scanning electron microscopy (FE-SEM). Fig. 1a shows the morphology of the synthesized $Bi_{13}S_{18}I_2$ by the reaction of excess thiourea to BiI_3 according to 4 : 1 molar ratio, showing that rod-like particles assembled in dandelion flower shapes. Elemental mapping shows the homogeneity of Bi, S and I across the particles (Fig. S1, ESI†). Energy dispersive spectroscopy (EDS) attached with SEM confirms that Bi, S and I are present according to the composition $Bi_{6.35}S_{9.12}I$, *i.e.*, $Bi_{12.71}S_{18.24}I_2$ (Fig. S2, ESI†). Fig. 1b shows the Rietveld refined powder X-ray diffraction (XRD) pattern of the synthesized bismuth sulfide iodide, which matches with trigonal $Bi_{13}S_{18}I_2$ in the *P*3 space group (ICSD 243731).[8] The estimated lattice parameters from the Rietveld refinement of $Bi_{13}S_{18}I_2$ are a = 15.703(4) Å and c = 4.035(1) Å with R_{exp} = 2.4920, R_{wp} = 7.1516, R_p = 5.5369, χ^2 = 1.694 and GOF = 2.869. The inset of Fig. 1b shows the crystal structure of the trigonal $Bi_{13}S_{18}I_2$. Fig. 1c shows the vis-NIR absorbance spectrum of the synthesized compound, showing the absorption of a complete visible range with a band gap calculated using the Kubelka–Munk function of 0.83 eV (inset Fig. 1c), which is consistent with previously reported values.[8] The thermal stability of the synthesized $Bi_{13}S_{18}I_2$ was characterized by thermogravimetric analysis (TGA) under a nitrogen atmosphere, which shows a single-step dissociation (Fig. 1d). After the thermal treatment, the obtained product was further characterized by XRD, which matches well with orthorhombic Bi_2S_3 (Fig. S3, ESI†).[5]

The morphology of the synthesized bismuth sulfide iodide obtained by reacting 1 mmol of thiourea with 1 mmol of BiI_3 is shown in Fig. 2a, showing a rod-like microstructure with a random arrangement, unlike $Bi_{13}S_{18}I_2$. Elemental mapping shows the homogeneity of Bi, S and I across the microstructure (Fig. S4, ESI†), which are present according to the average composition $BiS_{0.98}I_{1.03}$ (Fig. S5, ESI†). The observed reflections in the powder XRD pattern closely resemble those of orthorhombic BiSI in the *Pnma* space group (ICSD 023631) along with the secondary phase trigonal $Bi_{13}S_{18}I_2$ in the *P*3 space group (Fig. 2b). The estimated lattice parameters from the Le Bail refinement are a = 8.501(5) Å, b = 10.256(0) Å and c = 4.176(1) Å with R_{wp} = 0.0395, R_p = 0.0295, χ^2= 1.602 and GOF =1.27. The secondary phase of trigonal $Bi_{13}S_{18}I_2$ was also incorporated into the Le Bail refinement and its % mass contribution was found to be approx. 23%. Inset of Fig. 2b shows the crystal structure of orthorhombic BiSI. Fig. 2c shows the vis-NIR absorbance spectrum of the synthesized BiSI/$Bi_{13}S_{18}I_2$ with a calculated band gap of 1.59 eV by using Kubelka–Munk functions (inset Fig. 2c), which is close to the previously reported BiSI band gap value of 1.57–1.59 eV.[4] TGA analysis of the synthesized BiSI/$Bi_{13}S_{18}I_2$ in Fig. 2d shows two major steps in temperature-dependent dissociation. The TGA result is consistent with previous reports that indicate the formation of intermediate phase $Bi_{13}S_{18}I_2$ and Bi_2S_3 as the final product, while a few percent of weight loss at around 230 °C might be due to intriguing chemistry between BiSI and $Bi_{13}S_{18}I_2$.[7,15]

Based on our results, both sulfur-rich and sulfur-deficient compositions of mixed-anion bismuth-based compounds could be directly obtained by simply controlling the reactive sulfur concentration under identical experimental conditions. The presence of thiourea also ensures a reducing atmosphere. Because of a low boiling point and a high vapour pressure, ethanol was used for low temperature reactions. The use of

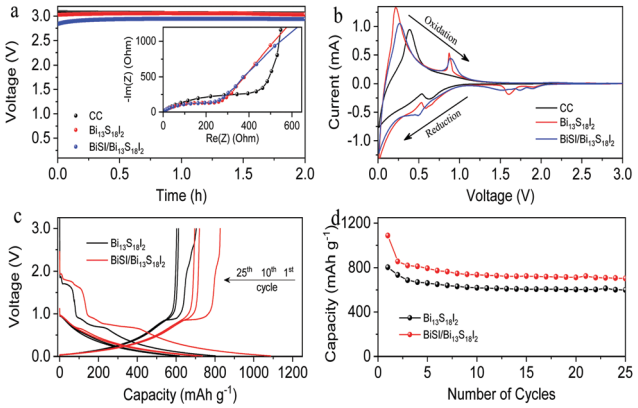

Fig. 3 (a) Open circuit voltages (OCVs) of the half-cells employing carbon cloth (CC), $Bi_{13}S_{18}I_2$, and BiSI/$Bi_{13}S_{18}I_2$ electrodes; (inset) electrochemical impedance spectroscopy (EIS) of the as-prepared cells prior to the electrochemical analysis. (b) Cyclic voltammetry (CV) curves of the cells measured at a scan rate of 0.2 mV s^{-1}. (c) Voltage profiles and (d) charge–discharge performance of the cells at a current density of 100 mA g^{-1}.

excess sulfur leads to sulfur-rich compositions, *i.e.*, $Bi_{13}S_{18}I_2$, while equivalent/less sulfur favours a sulfur deficient composition, *i.e.*, BiSI. Bismuth shows a high oxygen affinity and to avoid any kind of oxygen contamination, a reducing atmosphere in a non-aqueous solvent is recommended for bismuth chalcohalide synthesis. Thus, the presented facile synthesis of ternary Bi–S–I compounds by simply varying the sulfur concentration is favourable, which enables us to control the chemical composition under mild reaction conditions.

We demonstrated the performance of the synthesized $Bi_{13}S_{18}I_2$ and BiSI/$Bi_{13}S_{18}I_2$ as the anodes in LIBs by depositing the compounds onto a carbon cloth (CC) current collector. The 2032 type half-cells were assembled by employing lithium metal as the counter electrode and a commercial electrolyte of 1.0 molar $LiPF_6$ in an ethylene carbonate/dimethyl carbonate solution (1 : 1 vol%). Fig. 3a represents the open circuit voltages (OCVs) of the cells ranging from 2.9 to 3.1 V recorded for 2.0 hours prior to the electrochemical measurements, the stable OCVs indicate good compatibility of the electrodes as there is no self-discharge observed within the cells.[16] The electrochemical impedance spectroscopy (EIS) measurements (inset Fig. 3a) show comparable resistivity of $Bi_{13}S_{18}I_2$ and BiSI, *i.e.*, ~260 Ω. The observed resistivity value is much lower compared to that of the pristine CC (~440 Ω), as confirmed by the smaller semicircles of the cells employing $Bi_{13}S_{18}I_2$ and BiSI than that of pristine CC. Fig. 3b shows the cyclic voltammetry (CV) curves of the cells, recorded at a scan rate of 0.2 mV s^{-1} after the OCV and EIS measurements. Bismuth containing compounds are known for alloy formation with lithium.[17,18] The cathodic peaks in the CV curves (Fig. 3b) between 1.5 V and 1.9 V suggest the conversion of $Bi_{13}S_{18}I_2$ and BiSI/$Bi_{13}S_{18}I_2$ to metallic Bi upon the lithiation process,[17,18] which is confirmed by the formation of plateaus upon the first galvanostatic discharge of the corresponding electrodes in Fig. 3c. Cathodic peaks between 0.5 V and 0.6 V shown in Fig. 3b can be assigned to the alloying process of metallic Bi with Li.[17,18] The *ex situ* XRD analysis of the electrodes after discharging reveals that the conversion of $Bi_{13}S_{18}I_2$ and BiSI/$Bi_{13}S_{18}I_2$ results in Li_3Bi, and Li_3Bi along with LiBi, respectively, as presented in Fig. S6 (ESI†). Similar to the desodiation process in sodium-ion batteries from Na_3Bi to NaBi to Bi,[19] anodic scans (Fig. 3b) for $Bi_{13}S_{18}I_2$ and BiSI/$Bi_{13}S_{18}I_2$ show two peaks, one broad peak in the range of 0.2 V – 0.5 V and a second around 0.9 V, corresponding to delithiation of Li_3Bi to LiBi to Bi. The XRD patterns of charged $Bi_{13}S_{18}I_2$ and BiSI/$Bi_{13}S_{18}I_2$ match with that of metallic Bi, obtained after the dealloying process. The conversion is also consistent with the formation of plateaus of vthe oltage profiles upon charging at around 0.9 V (Fig. 3c).[17,18] Based on charge–discharge analysis, CV profiles, and XRD analysis, the reaction pathway in the $Bi_{13}S_{18}I_2$–Li and BiSI/$Bi_{13}S_{18}I_2$–Li cells during the discharge–charge process is shown below.

(I) Discharge process:

$$Bi_xS_yI_z \xrightarrow{+Li} xBi + yLi_2S + zLi \xrightarrow{+Li} xLi_3Bi$$

(II) Charge process:

$$Li_3Bi \xrightarrow{-Li} LiBi \xrightarrow{-Li} Bi$$

Fig. 3d shows that the cell employing BiSI/$Bi_{13}S_{18}I_2$ achieves an initial capacity of 1087 mA h g^{-1} and retains 703 mA h g^{-1} after 25 cycles, while the cell employing $Bi_{13}S_{18}I_2$ achieves capacities of 807 mA h g^{-1} and 601 mA h g^{-1}, respectively. Interestingly, both the ternary BiSI and $Bi_{13}S_{18}I_2$ compounds exhibit a stable cycling performance and achieve a higher capacity retention compared to the previously reported binary bismuth-based materials, as summarized in Table S1 (ESI†). To date, the application of bismuth-based materials as battery electrodes still lacks study, but researchers have found that these materials are promising for Li^+, Na^+, and K^+ storages.[9–14,17–22] Importantly, the class of ternary bismuth-based materials, such as Bi–S–I in this study and previously reported $BiSbS_3$,[11] suggest outstanding performance as battery electrodes over the binary bismuth-based materials and the state-of-the-art graphite anode (theoretical capacity of 372 mA h g^{-1}).[23,24] Furthermore, these materials merit further investigations, which include applications in other types of batteries, such as multivalent metal ion (*e.g.*, Zn^{2+}, Mg^{2+}, and Al^{3+}) battery systems.

In summary, we reported the controlled synthesis of $Bi_{13}S_{18}I_2$ and BiSI by simply tuning the sulfur concentration in a non-aqueous medium and demonstrate their potential as anode materials for rechargeable batteries. Our facile synthesis strategy enables variation of mixed-anion compounds beyond the Bi–S–I systems. Furthermore, the exploration of a new class of mixed-anion ternary $Bi_{13}S_{18}I_2$ and BiSI compounds as anode materials in LIBs paves the way to new research in the development of future electrodes for electrochemical energy storage systems, *e.g.*, Li^+, Na^+, K^+, Zn^{2+}, Mg^{2+}, and Al^{3+} batteries.

The authors are grateful to King Abdullah University of Science and Technology (KAUST) for the financial support. P. K. thanks Yuliar Firdaus for valuable suggestions.

Conflicts of interest

The authors declare no conflicts of interest.

References

1 H. Kageyama, K. Hayashi, K. Maeda, J. P. Attfield, Z. Hiroi, J. M. Rondinelli and K. R. Poeppelmeier, *Nat. Commun.*, 2018, **9**, 772.
2 M. Amsler, L. Ward, V. I. Hegde, M. G. Goesten, X. Yi and C. Wolverton, *Phys. Rev. Mater.*, 2019, **3**, 035404.
3 Daniel W. Davies, K. T. Butler, J. M. Skelton, C. Xie, A. R. Oganov and A. Walsh, *Chem. Sci.*, 2018, **9**, 1022–1030.
4 S. Li, L. Xu, X. Kong, T. Kusunose, N. Tsurumachi and Q. Feng, *J. Mater. Chem. C*, 2020, **8**, 3821–3829.
5 Z. S. Aliev, S. S. Musayeva, F. Y. Jafarli, I. R. Amiraslanov, A. V. Shevelkov and M. B. Babanly, *J. Alloys Compd.*, 2014, **610**, 522–528.
6 G. Miehe and V. Kupčík, *Naturwissenschaften*, 1971, **58**, 219.
7 W. Haase-Wessel, *Naturwissenschaften*, 1973, **60**, 474.
8 R. Groom, A. Jacobs, M. Cepeda, R. Drummey and S. E. Latturner, *Chem. Mater.*, 2017, **29**, 3314–3323.
9 L. Zhao, H.-H. Wu, C. Yang, Q. Zhang, G. Zhong, Z. Zheng, H. Chen, J. Wang, K. He, B. Wang, T. Zhu, X. C. Zeng, M. Liu and M.-S. Wang, *ACS Nano*, 2018, **12**, 12597–12611.
10 J. Ni, Y. Zhao, T. Liu, H. Zheng, L. Gao, C. Yan and L. Li, *Adv. Energy Mater.*, 2014, **4**, 1400798.
11 S. Wen, J. Zhao, J. Chen, J. Yang and J. Xu, *Dalton Trans.*, 2019, **48**, 10448–10454.
12 Y. Zhao, T. Liu, H. Xia, L. Zhang, J. Jiang, M. Shen, J. Ni and L. Gao, *J. Mater. Chem. A*, 2014, **2**, 13854–13858.
13 Y. Qin, Y. Zhang, J. Wang, J. Zhang, Y. Zhai, H. Wang and D. Li, *ACS Appl. Mater. Interfaces*, 2020, **12**, 42902–42910.
14 W. Sun, X. Rui, D. Zhang, Y. Jiang, Z. Sun, H. Liu and S. Dou, *J. Power Sources*, 2016, **309**, 135–140.
15 H. Sun, G. Yang, J. Chen, C. Kirk and N. Robertson, *J. Mater. Chem. C*, 2020, **8**, 13253–13262.
16 W. Wahyudi, Z. Cao, P. Kumar, M. Li, Y. Wu, M. N. Hedhili, T. D. Anthopoulos, L. Cavallo, L.-J. Li and J. Ming, *Adv. Funct. Mater.*, 2018, **28**, 1802244.
17 P. Kumari, K. Awasthi, S. Agarwal, T. Ichikawa, M. Kumar and A. Jain, *RSC Adv.*, 2019, **9**, 29549–29555.
18 C. Chen, P. Hu, X. Hu, Y. Mei and Y. Huang, *Chem. Commun.*, 2015, **51**, 2798–2801.
19 P. Xiong, P. Bai, A. Li, B. Li, M. Cheng, Y. Chen, S. Huang, Q. Jiang, X. H. Bu and Y. Xu, *Adv. Mater.*, 2019, **31**, 1904771.
20 C. Lu, Z. Li, L. Yu, L. Zhang, Z. Xia, T. Jiang, W. Yin, S. Dou, Z. Liu and J. Sun, *Nano Res.*, 2018, **11**, 4614–4626.
21 H. Liang, J. Ni and L. Li, *Nano Energy*, 2017, **33**, 213–220.
22 B. Hu, X. Wang, Q. Wei, H. Shu, X. Yang, Y. Bay, H. Wu, Y. Song and L. Liu, *J. Alloys Compd.*, 2013, **579**, 18–26.
23 J. Ming, Z. Cao, W. Wahid, M. Li, P. Kumar, Y. Wu, J.-Y. Hwang, M. N. Hedhili, L. Cavallo, Y.-K. Sun and L.-J. Li, *ACS Energy Lett.*, 2018, **3**, 335–340.
24 W. Wahyudi, V. Ladelta, L. Tsetseris, M. M. Alsabban, X. Guo, E. Yengel, H. Faber, B. Adilbekova, A. Seitkhan, A.-H. Emwas, M. N. Hedhili, L.-J. Li, V. Tung, N. Hadjichristidis, T. D. Anthopoulos and J. Ming, *Adv. Funct. Mater.*, 2021, **31**, 2101593.